Anisotropy of Electronic Spin Texture in the High-Temperature Cuprate Superconductor $Bi_2Sr_2CaCu_2O_{8+\delta}$

Wenjing Liu(刘文晶)[1,2], Heming Zha(查鹤鸣)[1,2], Gen-Da Gu(顾根大)[3], Xiaoping Shen(沈晓萍)[4], Mao Ye(叶茂)[1,2*], and Shan Qiao(乔山)[1,2,5*]

[1]*State Key Laboratory of Functional Materials for Informatics, Shanghai Institute of Microsystem and Information Technology, Chinese Academy of Sciences, Shanghai 200050, China*
[2]*Center of Materials Science and Optoelectronics Engineering, University of Chinese Academy of Sciences, Beijing 100049, China*
[3]*Condensed Matter Physics and Materials Science Department, Brookhaven National Laboratory, Upton, New York, 11973, USA*
[4]*State Key Laboratory of Surface Physics, Department of Physics, Fudan University, Shanghai 200433, China*
[5]*School of Physical Science and Technology, ShanghaiTech University, Shanghai 201210, China*

(Received 23 November 2022; accepted manuscript online 14 February 2023)

Seeking new order parameters and the related broken symmetry and studying their relationship with phase transition have been important topics in condensed matter physics. Here, by using spin- and angle-resolved photoemission spectroscopy, we confirm the helical spin texture caused by spin-layer locking in the nodal region in the cuprate superconductor $Bi_2Sr_2CaCu_2O_{8+\delta}$ and discover the anisotropy of spin polarizations at nodes along Γ–X and Γ–Y directions. The breaking of C_4 rotational symmetry in electronic spin texture may give deeper insights into understanding the ground state of cuprate superconductors.

DOI: 10.1088/0256-307X/40/3/037402

Ginzburg–Landau theory has revealed that phase transition and the appearance of the order parameter are accompanied by spontaneous symmetry breaking. Therefore, seeking new order parameters and the related broken symmetry and studying their relationship with phase transition has been an important topic in condensed matter physics for a long time. In the study of cuprates superconductors, scientists have found vital clues for broken symmetry for electronic states. The electrical resistance [1] and charge order [2] exhibit significant anisotropy, although the lattice structures are often weakly orthorhombic, with only about 1% orthorhombicity. This phenomenon is more common in iron-based superconductors and is known as the nematicity of the electronic state, [3,4] accompanied by the decreasing of rotational symmetry from C_4 to C_2. The symmetry breaking in the electronic state may be of great significance for understanding the ground states and complex phase diagrams of high T_c superconductors.

Angle-resolved photoemission spectroscopy (ARPES) is an excellent means of studying the electronic structure of solids. The band nesting and superstructure on the Fermi surface are often related to magnetic order or charge order and are important evidence of spontaneous symmetry breaking. For ARPES studies on cuprate superconductors, scientists have found that the tetragonal-to-orthogonal distortion of the crystal lattice is the main reason which leads to a $c(2 \times 2)$ shadow bands. [5–8] In bismuth-based cuprate superconductors, APRES measurements have revealed the anisotropic nested Fermi surface with incommensurate superstructures along specific direction. [9–11] It is well-known that the crystal structure of $Bi_2Sr_2CaCu_2O_{8+\delta}$ (Bi2212) has C_2 rotational symmetry rather than C_4, as the low-energy electron diffraction (LEED) pattern shown in Fig. 1(d). However, the origin of superstructure bands is still a debatable issue whether they are intrinsic properties of Cu–O_2 planes [12,13] or extrinsic due to diffraction of the Bi–O layers, [10,14] and it is still unclear whether the electronic structure breaks the C_4 symmetry or not. Besides energy and momentum, spin is also an important degree of freedom for electronic states. Recently, Gotlieb *et al.* [15] have revealed hidden spin-momentum locking in Bi2212. The spin texture of superstructure bands does not simply replicate that of the main band. The overall spin texture near the Fermi surface with a helical structure results from the spin-orbital coupling induced by local inversion symmetry breaking on a single Cu–O_2 plane. Until now, the spin polarizations at nodes along two orthogonal directions have not been compared directly, and the comparison is important for confirming the symmetry of the ground state.

The ability to probe energy, momentum, and spin of quasi-particles simultaneously makes spin- and angle-resolved photoemission spectroscopy (SARPES) an ideal technique to investigate the electronic spin texture in materials. In this Letter, by using ARPES and SARPES, we study the spin texture of the nearly optimal doped Bi2212 ($T_c = 90$ K) in the nodal region and confirm the hidden spin-momentum locking. The experimental results reveal the anisotropy of spin polarizations at nodes along different high symmetry axes with C_2 rotational symmetry while the dispersion and bandwidth of quasi-particles remain the same. The observed polarization along Γ–Y at

*Corresponding authors. Email: yemao@mail.sim.ac.cn; qiaoshan@mail.sim.ac.cn
© 2023 Chinese Physical Society and IOP Publishing Ltd

the node is about 8% and about twice as large as that along Γ–X. The anisotropy of the polarization indicates a symmetry break in the spin structure of the electronic state and gives insights into understanding the ground state of high T_c superconductors.

The cuprates have a similar ordered arrangement of slabs stacked along the c-axis. The conducting Cu–O_2 slabs are sandwiched between specific binding slabs consisting mainly of insulating layers of metal oxides. The electronic structure near the Fermi surface is mainly determined by the conducting Cu–O_2 slabs. BSCCO, like most cuprate superconductors, has a centrosymmetric lattice structure. Figure 1(b) shows the lattice structure of Bi2212. Two adjacent Cu–O_2 planes, shaded by the blue color, are separated by a Ca layer. The black arrows indicate the possible directions of the dipole fields, which leads to the spin-orbit coupling of the opposite signs on different layers, and this phenomenon is called hidden spin polarization or spin-layer locking.[15,16]

We study a nearly optimal doped Bi2212 with T_c = 90 K. Spin-integral and spin-resolved ARPES measurements were conducted with a homemade image-type spin detector consisting of a Scienta R3000 analyzer fitted with a multichannel very low electron energy diffraction (MCVLEED) spin polarimeter.[17] The spin polarimeter was more readily to measure the in-plane spin component than the out-plane spin component. The energy and angle resolutions are about 35 meV and 0.255°, respectively. The samples were cleaved *in situ* under an ultrahigh vacuum better than 1×10^{-10} Torr and all measurements were carried out at ~6 K. All the measurements were carried out by Xe (8.43 eV) light source except the Fermi surface in Figs. 1(a) and 2(a), which was measured with He Iα (21.2 eV).

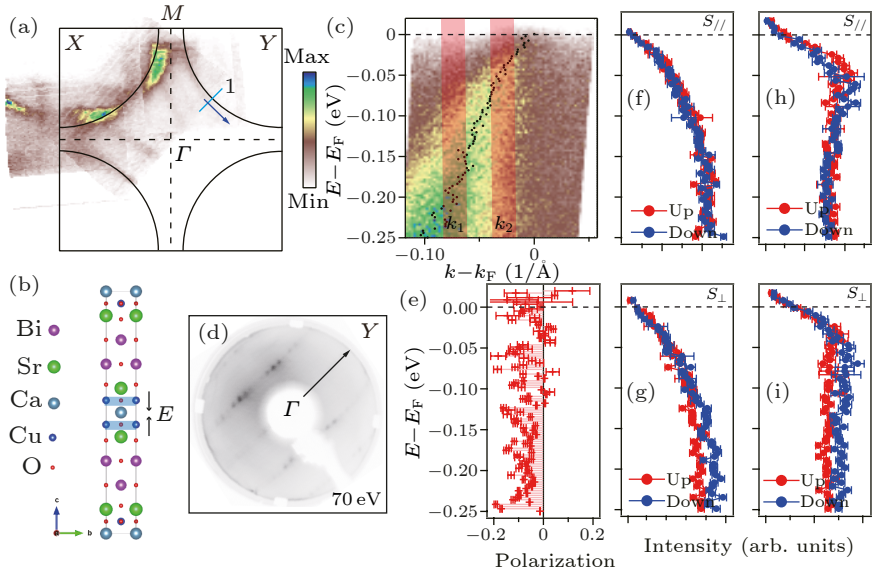

Fig. 1. The SARPES measurements along Γ–Y direction of optimal doping Bi2212. (a) The Fermi surface. The blue line indicates the position of cut 1 in reciprocal space. The blue arrow indicates the direction of spin. (b) The unit cell of Bi2212. The black arrows indicate the dipole fields caused by local inversion asymmetry on the Cu–O_2 plane. (c) Spin-integrated E–k image of cut 1 along Γ–Y directions. The red, transparent shaded area marks the locations of the spin-resolved EDCs. The band dispersion is indicated by a black dotted line. (d) LEED pattern of Bi2212 with the electronic kinetic energy being 70 eV. The arrow indicates the direction of the superstructure. (e) Spin polarization versus energy along the band dispersion. [(f), (g)] Spin-resolved EDCs at k_1 for spin components parallel ($S_{//}$) and perpendicular ($S_\perp$) to $K_{//}$. [(h), (i)] Spin-resolved EDCs at k_2 for $S_{//}$ and $S_\perp$.

In the MCVLEED spin polarimeter, a Fe(001)-$p(1\times1)$–O film grown on a MgO(001) was used as a spin filter.[17] The spin polarization is determined as $P^i = A^i/S_{\text{eff}} = 1/S_{\text{eff}}\cdot(I^i_+ - I^i_-)/(I^i_+ + I^i_-) = (I^i_\uparrow - I^i_\downarrow)/(I^i_\uparrow + I^i_\downarrow)$, where $S_{\text{eff}} = 0.30$ is the effective Sherman function determined by the measurements on the Bi/Si(111) sample, and I^i_+ and I^i_- are the intensities measured under opposite target magnetizations along i axis. $I^i_{\uparrow\downarrow} = (1\pm P^i)\cdot(I^i_+ + I^i_-)/2$ are the electron populations of opposite spins. The uncertainty $\delta I^i_\pm = \sqrt{I^i_\pm}$. The uncertainty over the spin polarization P^i is $\delta P^i = P^i\cdot\sqrt{\frac{(\delta I^i_+)^2+(\delta I^i_-)^2}{(I^i_+ + I^i_-)^2} + \frac{(\delta I^i_+)^2+(\delta I^i_-)^2}{(I^i_+ - I^i_-)^2}}$, and $\delta I^i_{\uparrow\downarrow} = I^i_{\uparrow\downarrow}\cdot\sqrt{\frac{(\delta P^i)^2}{(1\pm P^i)^2} + \frac{(\delta I^i_+)^2+(\delta I^i_-)^2}{(I^i_+ + I^i_-)^2}}$.

Figure 1(c) shows the band dispersion of nodal cut 1 along Γ–Y, and the spin-resolved energy distribution curves (EDCs) at k_1 and k_2 are shown in Figs. 1(f)–1(i). The black dotted line shows the positions of the Lorentz peaks by fitting the momentum distribution curves (MDCs). The experimental results clearly show that there is a nonzero in-plane spin component $S_\perp$ perpendicular to momentum and the spin component $S_{//}$ parallel to momentum is almost zero as shown in Fig. 1(a). The spin polarization caused by spin layer locking along the band dispersion [black dotted line in Fig. 1(c)] is extracted and plotted in Fig. 1(e). When calculating the polarization, the intensities are integrated over the bandwidth [shown in Fig. 3(c)].

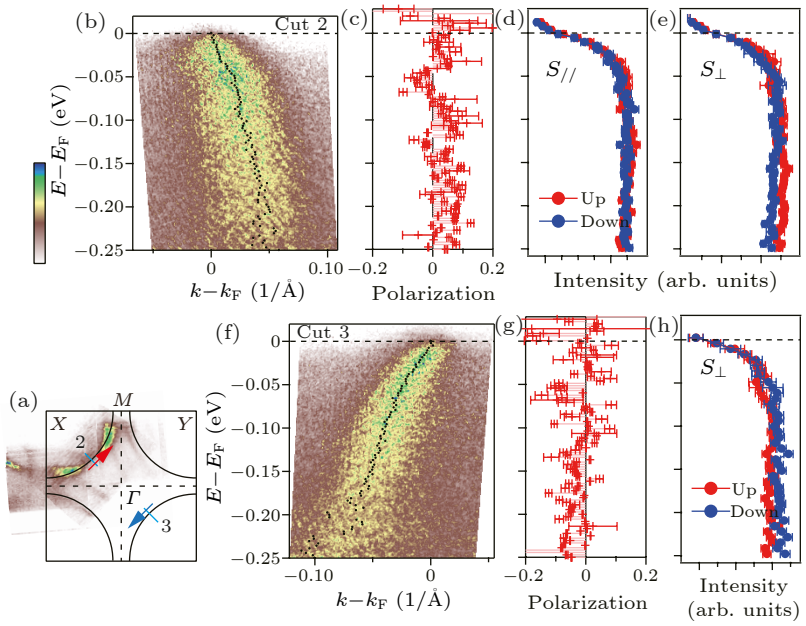

Fig. 2. The SARPES measurements along Γ–X direction of optimal doping Bi2212. (a) The Fermi surface. The positions of cuts 2 and 3 in reciprocal space are indicated by the blue solid line. The blue and red arrows indicate the directions of spin. [(b), (f)] Spin-integrated E–k image along nodal cuts 2 and 3. [(c), (g)] Spin polarization versus energy along the dispersion indicated by the black dotted line in (b) and (f). [(d), (e)] Spin-resolved EDCs of $S_{//}$ and $S_\perp$ for the nodal cut 2. (h) Spin-resolved EDCs of $S_\perp$ for cut 3. The spin-resolved EDCs are obtained by integrating the momentum range between [0, 0.1] and [−0.1, 0] for cuts 2 and 3, respectively.

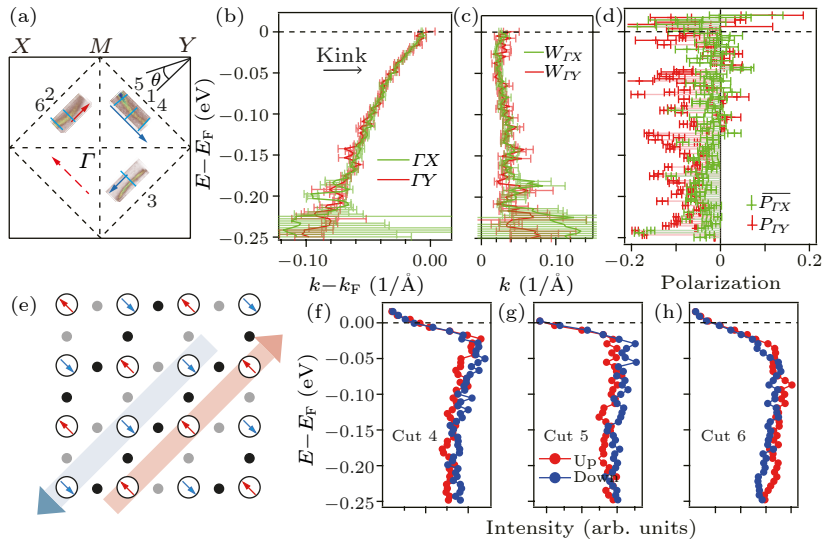

Fig. 3. Comparison of the band dispersion and spin polarizations along Γ–X and Γ–Y directions. (a) Fermi surface of Bi2212 and the schematic of the spin texture in the nodal region. The arrows illustrate the spin texture at the nodal area with its length indicating the magnitude of spin polarization. The dashed arrow is extrapolated from symmetry. (b) Band dispersions and (c) band width along Γ–X and Γ–Y directions extracted from Figs. 1(c) and 2(f) by fitting the MDCs with a Lorentz function. The black arrow indicates the kink at around −0.05 eV. (d) Spin polarization versus energy along the band dispersion at nodes along Γ–X and Γ–Y directions, where $P_{\overline{\Gamma X}} = (P^{\rm cut3}_{\Gamma X} - P^{\rm cut2}_{\Gamma X})/2$. (e) Schematic diagram of the local magnetic structure of an orthogonal phase [18,19] and a microscopic picture of polarization anisotropy. The black and grey solid dots represent oxygen atoms tilted up and down out of the plane, the circles represent copper atoms, and the arrows inside the circles represent local spins. The big arrows represent the hopping process along (110) directions. The SOC is stronger if the hopping direction is perpendicular to the local spin at Cu atoms. (f)–(h) Spin-resolved EDSs of $S_\perp$ at off-nodal cuts 4, 5, and 6.

The SARPES measurements at the nodes along Γ–X are shown in Fig. 2. The E–k spectrum of nodal cut 2 is shown in Fig. 2(b) and the corresponding spin-solved EDCs of $S_{//}$ and $S_\perp$ are shown in Figs. 2(d) and 2(e). Nonzero spin polarizations are also observed here with the spin directions indicated in Fig. 2(a). The spin polarizations along the band dispersion [black dotted line in Figs. 2(b) and 2(f)] are also extracted and plotted in

Figs. 2(c) and 2(g), and they reverse at $+k$ and $-k$ at nodes. It is ensured by time-reversal symmetry. However, the magnitude of polarization is smaller than that along Γ–Y direction.

The band dispersions and the band widths of the quasiparticles along Γ–X and Γ–Y directions [the black dotted lines in Figs. 1(c) and 2(f)] are almost the same as plotted in Figs. 3(b) and 3(c). The polarizations versus energy along the band dispersion at nodes along Γ–X and Γ–Y directions are plotted in Fig. 3(d) with $\bar{P_{\Gamma X}} = \frac{P_{\Gamma X}^{\rm cut3} - P_{\Gamma X}^{\rm cut2}}{2}$. It is clear that $P_{\Gamma Y} > \bar{P_{\Gamma X}}$. The spin polarizations are anisotropic and the rotational symmetry of the quasiparticle state is C_2 at nodes from our spin-resolved ARPES measurements. If it is assumed that the magnitudes of spin polarizations below the kink at -0.05 eV do not change with energy, then the polarizations of different energies can be averaged, and $\langle P_{\Gamma Y}\rangle$, $\langle \bar{P_{\Gamma X}}\rangle$ are 0.08 ± 0.01 and 0.036 ± 0.014, respectively. The t-test statistic of $P_{\Gamma Y}$ and $\bar{P_{\Gamma X}}$ is 21.7 (data number $n = 73$), and the probability that the two sets of data belong to the same distribution is only about 10^{-8}.

The helical spin texture at the nodal region observed in our work can be explained by the hidden spin-momentum locking effect. Gotlieb *et al.*[15] have first revealed this phenomenon in the overdoped Bi2212 with $T_{\rm c} = 58$ K. However, there are three main differences between our experimental results and theirs. First, the polarization at node along Γ–Y increases up to 40% at higher binding energy in their works and is much larger than our results. Second, the reversal of $S_\perp$ off nodes was not been observed in our experiments. The spin-resolved EDCs of $S_\perp$ at off-nodal cuts 4, 5, and 6 with $\theta = 13^\circ$ [θ is defined in Fig. 3(a)] are shown in Figs. 3(f)–3(h), and $S_\perp$ does not change signs along the fermi arc in nodal region. The third difference is that they did not measure the spin polarizations at node along Γ–X and assumed the presence of four-fold rotation symmetry. Since they used a 6 eV pulsed laser source with s-polarized photons, the first two differences are most likely due to matrix element effects caused by the selection rules of polarized light.[20,21] Because the ultraviolet Xe (8.43 eV) light source we used is unpolarized, and the geometry setup always remained unchanged during the experiments except for the rotation of the sample, the experimental results should reflect the property of the initial states.

The observation of the anisotropic spin polarization at nodes is clear evidence that the rotational symmetry of the quasi-particles there is C_2. Experimental and theoretical works have revealed the complex spin orders in cuprate superconductors[19,22,23] and their magnetic structure is related to Dzyaloshinskii–Moriya interaction and the buckling of the Cu–O_2 plane.[18] Here we propose a microscope picture to understand the origin of polarization anisotropy as illustrated in Fig. 3(e). The SOC is stronger when the hopping direction is perpendicular to the local spin at Cu atoms since $H_{\rm SOC} = \alpha(\nabla V \times p)\cdot\sigma$. The anisotropic polarization could be the result of the combined action of SOC and the spin order in the Cu–O_2 plane. However, in the superconducting regime, the spin has large fluctuations rather than forms a static spin order, the origin of the anisotropic polarization in the nodal region needs further study.

In conclusion, by using spin- and angle-resolved photoemission spectroscopy, we have observed the helical spin texture with a large anisotropic polarization in the nodal region in optimal doped Bi2212. The observation of C_4 rotational symmetry breaking in electronic spin states gives deeper insights into understanding the ground state of cuprate superconductors.

Acknowledgements. This work was supported by the National Natural Science Foundation of China (Grant Nos. U1632266, 11927807, and U2032207) and the National Key R&D Program of China (Grant No. 2017YFA 0305400). The work at BNL was supported by the US Department of Energy, Office of Basic Energy Sciences (Grant Nos. DOE-sc0012704).

References

[1] Ando Y, Segawa K, Komiya S *et al.* 2002 *Phys. Rev. Lett.* **88** 137005
[2] Lawler M, Fujita K, Lee J *et al.* 2010 *Nature* **466** 347
[3] Coldea1 A I and Watson M D 2018 *Annu. Rev. Condens. Matter Phys.* **9** 125
[4] Wen C H P *et al.* 2016 *Nat. Commun.* **7** 10840
[5] Nakayama K, Sato T, Dobashi T *et al.* 2006 *Phys. Rev. B* **74** 054505
[6] M, Santoso I, Huang Y, Siu W K *et al.* 2006 *Phys. Rev. Lett.* **96** 107007
[7] Koitzsch, Borisenko S V, Kordyuk A A *et al.* 2004 *Phys. Rev. B* **69** 220505(R)
[8] Singh D J and Pickett W E 1995 *Phys. Rev. B* **51** 3128
[9] Aebi P, Osterwalder J, Schwaller P *et al.* 1994 *Phys. Rev. Lett.* **72** 2757
[10] Ding H, Bellman A F, Campuzano J C *et al.* 1996 *Phys. Rev. Lett.* **76** 1533
[11] Mesot J, Norman M R, Ding H *et al.* 1999 *Phys. Rev. Lett.* **82** 2618
[12] Liu J, Zhao L, Gao Q *et al.* 2019 *Chin. Phys. B* **28** 077403
[13] Gao Q, Yan H, Liu J *et al.* 2020 *Phys. Rev. B* **101** 014513
[14] Osterwalder J, Aebi P, Schwaller P *et al.* 1995 *Appl. Phys. A* **60** 247
[15] Gotlieb K, Lin C Y, Serbyn M *et al.* 2018 *Science* **362** 1271
[16] Zhang X W, Liu Q H, Luo J W *et al.* 2014 *Nat. Phys.* **10** 387
[17] Ji F H, Shi T, Ye M *et al.* 2016 *Phys. Rev. Lett.* **116** 177601
[18] Koshibae W, Ohta Y, and Maekawa S 1993 *Phys. Rev. B* **47** 3391
[19] Tranquada J M, Sternlieb B, Axe J D *et al.* 1995 *Nature* **375** 561
[20] Manzke R, Müller R, Janowitz C, Schneider M, Krapf A, and Dwelk H 2001 *Phys. Rev. B* **63** 100504
[21] Yaji K, Kuoda K, Toyohisa S *et al.* 2017 *Nat Commun.* **8** 14588
[22] Fong H, Bourges P, Sidis Y *et al.* 1999 *Nature* **398** 588
[23] Zheng B X, Chung C M, Corboz P *et al.* 2017 *Science* **358** 1155